The American Journal of Pathology, Vol. 186, No. 2, February 2016

The American Journal of
PATHOLOGY
ajp.amjpathol.org

CARDIOVASCULAR, PULMONARY, AND RENAL PATHOLOGY

Exocytosis of Endothelial Lysosome-Related Organelles Hair-Triggers a Patchy Loss of Glycocalyx at the Onset of Sepsis

Joseph A. Zullo,* Jie Fan,† Tala T. Azar,† Wanyi Yen,† Min Zeng,† Jun Chen,* Brian B. Ratliff,* Jun Song,*‡ John M. Tarbell,† Michael S. Goligorsky,* and Bingmei M. Fu†

From the Department of Medicine, Pharmacology and Physiology, New York Medical College, Valhalla, New York; the Department of Biomedical Engineering,† The City College of the City University of New York, New York, New York; and the Department of Anesthesiology,‡ Ulsan Medical College, Seoul, Republic of Korea*

Accepted for publication October 16, 2015.

Address correspondence to Bingmei M. Fu, Ph.D., Department of Biomedical Engineering, The City College of the City University of New York, 160 Convent Ave, New York, NY 10031; or Michael S. Goligorsky, M.D., Ph.D., Department of Medicine, Pharmacology and Physiology, New York Medical College, Basic Sciences Bldg, 15 Dana Rd, Valhalla, NY 10595. E-mail: fu@ccny.cuny.edu or michael_goligorsky@nymc.edu.

Sepsis is a systemic inflammatory syndrome induced by bacterial infection that can lead to multiorgan failure. Endothelial surface glycocalyx (ESG) decorating the inner wall of blood vessels is a regulator of multiple vascular functions. Here, we tested a hypothesis that patchy degradation of ESG occurs early in sepsis and is a result of exocytosis of lysosome-related organelles. Time-lapse video microscopy revealed that exocytosis of Weibel-Palade bodies and secretory lysosomes occurred a few minutes after application of lipopolysaccharides to endothelial cells. Two therapeutic maneuvers, a nitric oxide intermediate, NG-hydroxy-L-arginine, and culture media conditioned by endothelial progenitor cells reduced the motility of lysosome-related organelles. Confocal and stochastic optical reconstruction microscopy confirmed the patchy loss of ESG simultaneously with the exocytosis of lysosome-related organelles and Weibel-Palade bodies in cultured endothelial cells and mouse aorta. The loss of ESG was blunted by pretreatment with NG-hydroxy-L-arginine or culture media conditioned by endothelial progenitor cells. Moreover, these treatments resulted in a significant reduction in deaths of septic mice. Our data support the hypothesis assigning to stress-induced exocytosis of these organelles the role of a hair-trigger for local degradation of ESG that initiates leukocyte infiltration, increase in vascular permeability, and partially accounts for the later rates of morbidity and mortality. *(Am J Pathol 2016, 186: 248–258; http://dx.doi.org/10.1016/j.ajpath.2015.10.001)*

Sepsis is a systemic inflammatory syndrome induced by bacterial infection that can lead to multiorgan failure. It afflicts >700,000 individuals annually in the United States alone, has mortality rates of 30%, and is the 11th leading cause of death. One of the key molecular causes of Gram-negative septicemia is endotoxin that consists of lipopolysaccharides (LPSs) bound with high affinity to LPS-binding glycoprotein. Complex LPS-binding glycoprotein is recognized by cognate receptor Toll-like receptor 4 and co-receptor CD14 on monocytes/macrophages and endothelial cells.[1] Considering the systemic nature of septicemia, vascular endothelium represents the first line of exposure to bacterial endotoxins.[2] It responds to endotoxins with a complex system of danger signals, which are chronologically sequenced and spatially propagated.[3] Functionally, these waves of danger signaling tend to secure proper organismal responses, both proinflammatory and anti-inflammatory.

Among the earliest responses of activated endothelial cells to endotoxin are exocytosis of Weibel-Palade bodies (WPBs) and secretory lysosomes.[4] WPBs are rod-shaped members of lysosome-related organelles (0.2 μm by 2 to 3

Supported by NIH grants DK54602, DK052783, and DK45462 (M.S.G.), SC1CA153325 (B.M.F.), and R01HL094889 (J.M.T. and B.M.F.); American Heart Association grant 12SDG9080006 (B.B.R.); American Society of Nephrology grant 010973-101 (B.B.R.); and The New York Community Trust - Renal Clinical Fund (B.B.R.).

J.A.Z. and J.F. contributed equally to this work.

Disclosures: None declared.

http://dx.doi.org/10.1016/j.ajpath.2015.10.001

μm in size) characteristic to endothelial cells and containing an array of proteins, peptides, and cytokines, which can be released emergently on demand. The endothelial lysosomes contain acid/secretory sphingomyelinase, glycohydrolases, cathepsins, fucosidase, phosphatases, heparan sulfate (HS) sulfatase, among others, but mechanisms of exocytosis of lysosome-related organelles have only been partially elucidated.

Endothelial surface glycocalyx (ESG) represents a superficial layer that consists of glycoproteins, proteoglycans, and glycosaminoglycans. Because of its unique location, this structure provides a passive barrier to water and solute transport, the interaction between circulating cells and the endothelial cells that form the inner wall of blood vessels, serves as a sensor of mechanical forces, such as shear stress and pressure, and represents a shielding instrument for cell surface receptors to prevent their hyperactivation.[5,6] This structure is, however, quite vulnerable and tends to disintegrate after application of various stressors, such as endotoxins, ischemia/hypoxia/reperfusion, oxidative stress, among others. Damage to and modification of the ESG are observed in many diseases, including diabetes, ischemia, myocardial edema, chronic infectious diseases, atherosclerosis, and tumor metastasis.[5–11] The disintegration of this structure predisposes to leukocyte adhesion, emigration, and tissue infiltration by polymorphonuclear cells, monocyte/macrophages, and lymphocytes. It also leads to hyperactivation of plasma membrane receptors by unhindered availability of ligands and further activation of danger signaling by endothelial cells.

Until now, the ESG remained poorly studied because of difficulties in preserving its structure on tissue fixation, limited number of experimental tools for its visualization, and requirements for an ultra-high resolution microscope. Therefore, there is no confidently chartered time course of damage and disintegration of ESG. Yet, the precise chronology of the loss of ESG is of critical significance, because it determines whether and to what extent the loss of glycocalyx is involved in the early pathogenic steps of systemic inflammatory response or only in its maintenance or in both. We hypothesized that exocytosis of WPBs and lysosomes, being an early response of endothelial cells to endotoxin, results in the focal disintegration of ESG. This singular event hair-triggers an avalanche of secondary pathologic processes, such as attraction of leukocytes and platelets, thrombosis, increased vascular permeability. The proof of this hypothesis lies in the demonstration of two key facts, namely, that exocytosis of WPBs and lysosomes does indeed trigger the initial loss of glycocalyx and that maneuvers directed toward preservation of glycocalyx improve the course of sepsis and overall survival. The recent discovery and implementation of the stochastic optical reconstruction microscopy (STORM) offered us a unique opportunity to detect the integrity of glycocalyx at the molecular resolution. Data presented herein support the validity of this hypothesis.

Materials and Methods

Cell Culture

Immortalized human umbilical vein endothelial cells (HUVECs; ATCC, Manassas, VA) and bEnd3 mouse brain microvascular endothelial cells (ATCC) were used in these studies. Cells were propagated in Dulbecco's modified Eagle's medium (DMEM) supplemented with 10% fetal bovine serum, 1% penicillin, and 50 μg/mL streptomycin, and 2 mmol/L L-glutamine under conditions of 37°C and 5% CO_2. Cells were seeded onto 50 μg/mL fibronectin-coated 35-mm glass-bottom culture dishes with 14-mm No.1.5 coverslips (Mat Tek Corp., Ashland, MA) at a density of 4×10^4 cells/mL and cultured until confluence. HUVECs were incubated with 50 to 75 nmol/L of LysoTracker Red (Invitrogen, Carlsbad, CA), in prewarmed (37°C) DMEM with 10% fetal bovine serum and 1% penicillin and streptomycin medium at 37°C for 30 minutes. After removing the medium, phenol red-free DMEM with 10% fetal bovine serum was added. Endothelial progenitor cells (EPCs) were isolated from developmental age embryonic day 7.5 to 7.8 murine embryos and generously provided by Dr. Antonis K. Hatzopoulos (Vanderbilt University, Nashville, TN).[12] EPCs were cultured in DMEM supplemented with 20% fetal bovine serum, 0.1 mmol/L β-mercaptoethanol, 1 mmol/L minimum essential amino acid at 37°C in 5% CO_2.

Animal Sepsis Models

The animal study protocol was in accordance with the NIH *Guide for the Care and Use of Laboratory Animals*[13] and approved by the Institutional Animal Care and Use Committee. For cecal ligation puncture (CLP) to induce sepsis, male mice (C57/BL6 age, >16 weeks) under isoflurane anesthesia had the cecal tip ligated with 4-0 silk suture. The cecum was punctured twice with a 21-guage needle, then gently squeezed. Wound was sutured, and mice were closely monitored by investigators with the use of a video camera.

In Vivo Endothelial Progenitor Cell Implantation

HA-hydrogels (Glycosan Biosystems, Salt lake City, UT) embedded with EPCs were implanted subcutaneously in the ears of sedated mice, as we reported previously.[14] Implantation of hydrogels occurred during the CLP and LPS *in vivo* procedures. A total of 1 million cells were delivered to each mouse. Ear implants were injected with 300 U/mL collagenase (Sigma-Aldrich, St. Louis, MO) and 100 U/mL hyaluronidase (Sigma-Aldrich) to permit mobilization of embedded cells immediately after the CLP procedure.

Immunofluorescence Staining of Cultured Cells

The cell monolayers were quickly washed with phosphate-buffered saline (PBS) and fixed with 2% paraformaldehyde/0.1% glutaraldehyde for 20 minutes, followed by 0.1% $NaBH_4$ for approximately 7 minutes at room temperature. After washing three times with PBS, the cells were blocked with 2% goat serum for 30 minutes, followed by an overnight incubation at 4°C with monoclonal primary antibody for HS (dilution 1:100; 10E4 epitope; AMS Biotechnology, Abingdon, United Kingdom) and von Willebrand factor (vWF)-labeled WPBs (vWF/WPBs; dilution 1:100; Dako Denmark A/S, Glostrup, Denmark). After washing three times with PBS, the cells were incubated for 1 hour at room temperature with the fluorescence-conjugated secondary antibody. Alexa Fluor 488-conjugated secondary antibody to HS and 20 μmol/L fluorescein isothiocyanate-conjugated Triticum vulgaris lectin (fluorescein isothiocyanate−wheat germ agglutinin; Sigma-Aldrich) were used for confocal microscopy, and Alexa Fluor 647-labeled and ATTO 488-labeled secondary antibodies to HS and vWF/WPBs were used for STORM, respectively, followed by washes three times.

Cathepsin Detection

Magic Red Cathepsin detection kit with the use of the fluorophore cresyl violet (Immunochemistry Technologies, Bloomington, IN) was used to detect cathepsin B in the media of cultured cells. In brief, cells were grown to 80% to 90% confluence in phenol-free complete media, before adding 5 μg/mL LPS. Media were collected and incubated with Magic Red Cathepsin detection kit at room temperature for 15 minutes. Fluorescence was detected at excitation/emission of 592/628 nm with the use of a Biotek synergyHT microplate reader and analyzed with the companion software (Gen5 version 1.11; Biotek, Winooski, VT).

Immunofluorescence Staining of Intact Blood Vessels

We imaged the ESG on the aorta of male C57BL/6 mice (The Jackson Laboratory, Bar Harbor, ME). The detailed animal preparation was described in our previous study.[15] After anesthesia, the mice were perfused with cold 1% bovine serum albumin-PBS to remove the blood and perfusion-fixed with 2% paraformaldehyde. Then the aorta was cut into approximately 1-cm long rings or prepared *en face* with a longitudinal cut. After washing with the PBS, the aortic rings were blocked for 30 minutes with 1% bovine serum albumin saponin solution. Then the aorta segments were incubated with mouse anti-HS antibody and anti-vWF/WPBs overnight. After a brief wash with PBS, the specimens were blocked for 30 minutes and incubated with the Alexa Fluor 488-labeled and Alexa Fluor 647-labeled goat anti-mouse IgG for 2 hours, respectively, to anti-HS and anti-vWF/WPBs, followed by washes three times. Longitudinal segments for *en face* preparations used fluorescein isothiocyanate−wheat germ agglutinin as an alternate to the anti-HS antibody. Samples were incubated with 20 μmol/L fluorescein isothiocyanate−wheat germ agglutinin for 30 minutes at 4°C, then washed three times with PBS immediately before imaging.

Treatment of HUVECs with LPS, NOHA, and EPC-CM

For fluorescence imaging, cells were cultured in fibronectin-coated 60-mm glass-bottom cell culture dishes (MatTek Corp.) until confluence (2 to 3 days). To prepare EPC-conditioned medium (EPC-CM), EPCs were cultured in 60-mm cell culture dishes for 24 hours. After 24 hours, DMEM was replaced with serum- and phenol-free medium for an additional 24 hours of incubation. Thus, prepared CM was filtered with sterile cell strainer, divided into aliquots, and stored until use at −80°C.

Individual HUVECs were selected and monitored by time-lapse videomicroscopy before and after application of 5 μg/mL LPS. For the LPS + NG-hydroxy-L-arginine (NOHA; Sigma-Aldrich) group, 100 μg/mL NOHA was added 20 minutes before applying 5 μg/mL LPS in the medium. For the EPC-CM10 and EPC-CM50 groups, 1:10 or 1:50 dilutions of EPC-CM were added 20 minutes before applying 5 μg/mL LPS in the medium. NOHA and EPC-CM were selected as treatment options on the basis of the previous demonstration of the nitric oxide donor's ability to curtail exocytosis of lysosome-related organelles[16] and our previous demonstration of the therapeutic activity of EPCs against septic vascular damage.[3]

In another group of experiments, bEnd3 cells were incubated with 50 nmol/L LysoTracker Red for 15 minutes. After a wash with a fresh medium, 5 μg/mL LPS was added for 10, 30, and 60 minutes. Then the cells were fixed with 3.7% paraformaldehyde, immunolabeled with primary anti-HS and then Alexa Fluor 488-labeled secondary antibody and observed by confocal microscopy.

Oxidative Stress Detection

Dihydroethidium fluorescence intensity changed after LPS treatment. HUVECs were cultured to confluence, labeled with dihydroethidium, and treated with LPS at concentrations that ranged from 0 to 10 μg/mL. The oxidation of dihydroethidium was evaluated by fluorescent plate reader with excitation/emission wavelengths set at 485 ± 20/620 ± 40 nm. The fluorescence intensity of various treatment groups at each time point was normalized against the unlabeled group for each time point.

Image Acquisition and Analysis of Lysosomal Trafficking

A Nikon Y-FL epifluorescence intravital microscope (Nikon Inc., Melville, NY) equipped with an intensified Cool SNAP

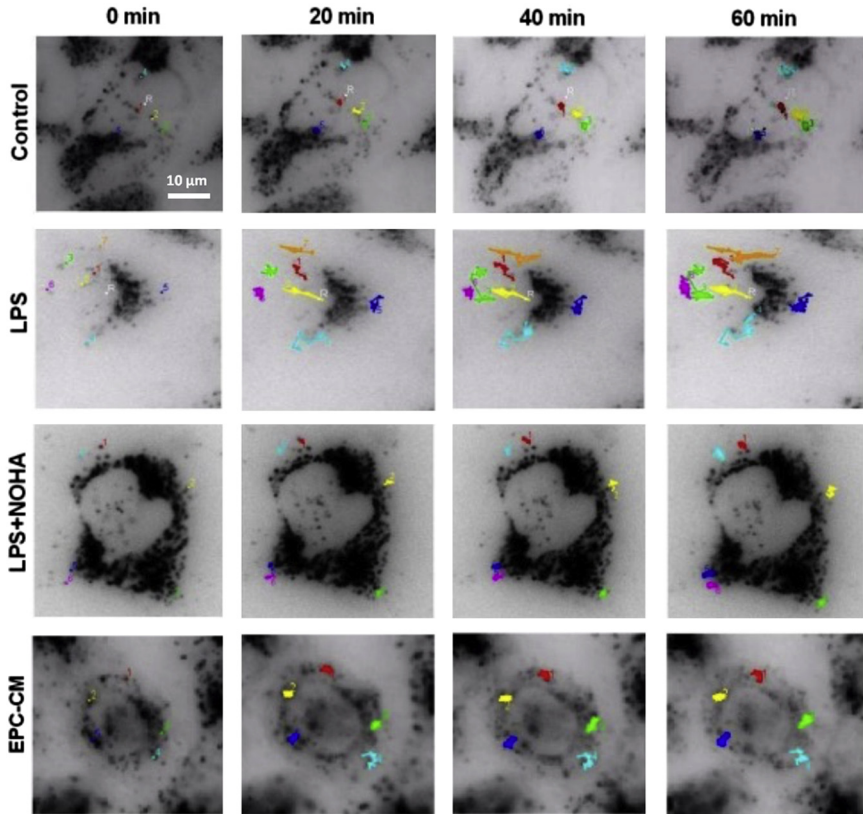

Figure 1 Representative time-lapse images of endothelial cells with labeled lysosomes. HUVECs were loaded with LysoTracker, incubated in serum-containing, phenol-free medium, and imaged with intravital videomicroscopy. Individual frames were selected from a time-lapse series obtained before and after application of LPS at the concentration of 5 μg/mL. For better visualization, all images were converted into negatives. Tracking of individual lysosomes is identified in different colors. Note that LPS induce a dramatic increase in lysosomal motility, which was curtailed by coapplication of EPC-CM or a nitric oxide donor, NOHA. Scale bar = 10 μm. CM, conditioned medium; EPC, endothelial progenitor cell; HUVEC, Human umbilical vein endothelial cell; LPS, lipopolysaccharide; NOHA, NG-hydroxy-L-arginine.

HQ tube camera (Photometrics, Tucson, AZ) and 60× Nikon Plan Apo objective was used for microscopy and image acquisition. Intravital videomicroscopy was performed over a time period of 120 minutes with a time-lapse interval set to 1 minute. Fluorescence was recorded, and fluorescence intensity was quantified for lysosomal particles in the cells with the use of MetaVue software version 6 (Universal Imaging, Downingtown, PA).

Lysosomal particle/point tracking analysis and measuring of lysosomal trajectories used the ImageJ software version 1.45m (NIH, Bethesda, MD; *http://imagej.nih.gov/ij*) with plugin Manual Tracking (Fabrice Cordelières, Institut Curie, Orsay, France). The lysosomes were selected from a large pool at random and with the only criterion that the candidate lysosome could be tracked unambiguously throughout the session. For example, two neighboring lysosomes in close proximity within the same plane could not be differentiated from each other. If this event occurred during the tracking, both lysosomes were excluded from analysis. Automation was attempted, using computerized particle tracking; however, results were inconsistent and subpar compared with manual tracking. Each lysosome was recorded in intervals of 2 minutes with the use of time-lapse video microscopy. All images were converted into negatives for better visualization. All data were expressed as means ± SEM. Differences in distances between groups at every time point were analyzed by two-way repeated measures analysis of variance, with time and groups as variables, and followed by the Holm-Sidak test for multiple comparisons. Comparison of trajectories among group differences tested by one-way analysis of variance, followed by the Holm-Sidak multiple comparison test. $P < 0.05$ was regarded as statistically significant.

Confocal and STORM Microscopy of Glycocalyx *ex Vivo* and *in Vitro*

Confocal Microscopy

We used a Zeiss LSM 710/510 confocal microscope (Carl Zeiss, Jena, Germany) with 63×/NA1.4 or 40×/NA1.3 objective lens to image the ESG of endothelial monolayers *in vitro* and mouse aorta *ex vivo* that were fixed and mounted on a coverslip. With the use of a motorized substage on the confocal microscope, z-stack images were generated of the cell monolayers and vessels. As described by Yen et al,[15] stacked confocal images were reconstructed and analyzed by ImageJ to quantify changes in ESG, lysosome, and vWF/WPBs distribution in cell monolayers and vessels.

Two-Dimensional Circle Packing ImageJ Algorithm

The algorithm created space-filling ellipses and circles to highlight areas depleted of glycocalyx. The automatized process used ImageJ. Briefly, a 63× confocal image was first converted to monochromatic, made into binary, and

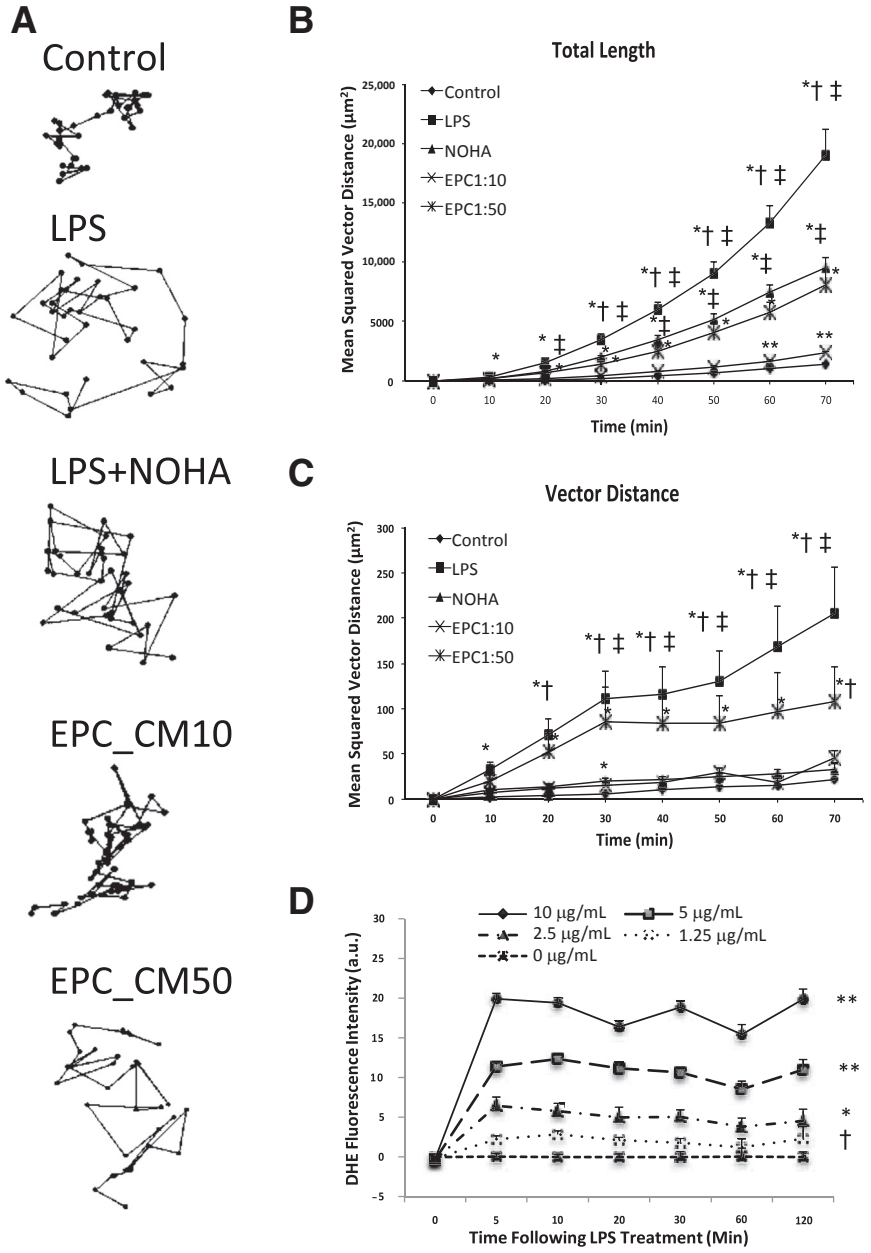

Figure 2 Trace, total length, and vector length of lysosomal exocytosis in iHUVECs and DHE fluorescence intensity. **A:** Representative and normalized XY-position traces of labeled lysosomes tracking over 60 minutes. The trajectories of peripheral lysosomes show significantly longer tracks in LPS, LPS + NOHA, and EPC-CM10 and EPC-CM50 groups. **B** and **C:** Individual organelles were randomly selected from a time-lapse series obtained before and after application of LPS, NOHA, and EPC-CM. In control, movements were non-vectorial. After LPS, lysosomal movement became more dynamic and directional. When nitric oxide donor NOHA or EPC-CM was used for pretreatment before LPS, lysosomal movements were reduced. **D:** DHE fluorescence intensity after LPS treatment of cultured HUVECs. Data are expressed as means ± SEM. $n = 4$ to 5 per group and 30 lysosomal particles per cell (**B** and **C**); $n = 12$ for 10 and 2.5 μg/mL groups (**D**); $n = 6$ for other tested groups (**D**). $^{*}P < 0.05$ versus total trajectory (**B** and **C**); $^{\dagger}P < 0.05$ versus control (**B** and **C**); and $^{\ddagger}P < 0.05$ versus LPS + NOHA and EPC-CM10 and EPC-CM50 (**B** and **C**), differences tested by one-way analysis of variance followed by the Holm-Sidak multiple comparison test. $^{*}P < 0.05$, $^{**}P < 0.01$ versus all lower LPS treatment group(s) at indicated times within each time point (**D**); $^{\dagger}P < 0.05$ versus no LPS (**D**). CM, conditioned medium; DHE, dihydroethidium; EPC, endothelial progenitor cell; iHUVEC, immortalized human umbilical vein endothelial cell; LPS, lipopolysaccharide; NOHA, NG-hydroxy-L-arginine.

then processed with the use of a watershed transformation. The results allowed for large cell populations to be analyzed consistently, effectively, and without bias. All functions pertaining to the algorithm are inherent to ImageJ.

STORM

We used a three-dimensional multicolor ultra-high resolution Nikon-STORM system to image the ESG and vWF/WPBs of bEnd3 monolayers. The system consisted of a Nikon TiE Inverted Microscope stand with internal encoded Z-drive with 25-nm resolution and Nikon Perfect Focus System. The high magnification and high numerical aperture objective 100×/NA1.494 (oil immersion) enables super resolution images by offering high transmission and superior chromatic aberration correction throughout a wide wavelength range, from near-ultraviolet to near-infrared. The secondary antibodies conjugated with the photo switchable dyes, Alexa Fluor 647 and ATTO 488, were used to identify HS of the ESG and vWF, respectively.

Survival Analysis

Kaplan-Meyer survival curves were generated with male C57BL/6 mice subjected to CLP over a 72-hour observation period. Double-blind randomization and administration of treatment was performed for healthy controls, NOHA, EPC-CM, CLP, CLP + EPC-CM, and CLP + NOHA. Mice in each treatment group ($n = 10$ each) were monitored at hourly intervals and provided water and food ad lib.

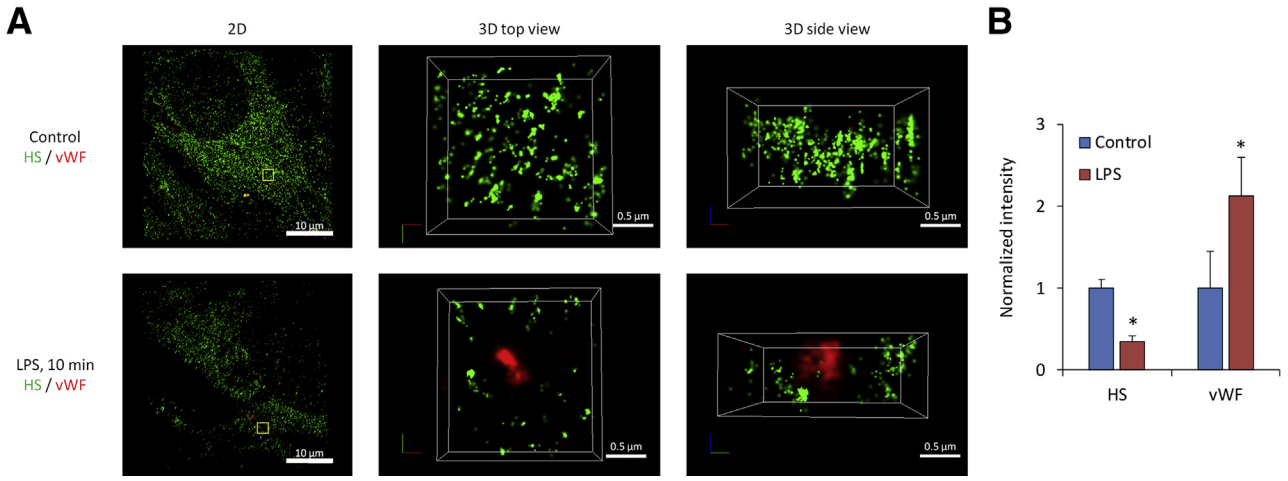

Figure 3 Representative STORM-acquired images of anti-HS—labeled ESG and vWF distribution in control and 10 minutes after LPS. **A:** The **left panel** shows 2D images of a region of approximately 40 μm × 40 μm in a sample. An enlarged top view of a **yellow box** (approximately 2 μm × 2 μm) in the **left panel** is shown in the **middle panel** and its side view in the **right panel.** The bEnd3 EC surface is at the bottom of the side view. **Upper panels** are for the control and bottom ones after 10 minutes of LPS treatment. **B:** Relative intensity of anti-HS and vWF-labeled WPBs after 10 minutes of LPS treatment compared with the control. Data are expressed as means ± SD. $n = 3$ samples each for the control and LPS treatment. Three regions of approximately 40 μm × 40 μm were observed in each sample and 10 subregions of approximately 2 μm × 2 μm were randomly selected and analyzed in each region. *$P < 0.05$ versus the control. EC, endothelial cell; ESG, endothelial surface glycocalyx; HS, heparan sulfate; LPS, lipopolysaccharide; STORM, stochastic optical reconstruction microscopy; vWF, von Willebrand factor; WPB, Weibel-Palade body; 2D, two-dimensional; 3D, three-dimensional.

Statistical Analysis

Studies were sufficiently powered to detect significant changes in fluorescence imaging. A calculated biological replica of $n = 8$ was sufficient to detect differences at $\alpha = 0.05$, powered to 0.9 (PASS software version 12.0.10; NCSS version 9.0.15; NCSS Statistical Software, Kaysville, UT). Hypothesized means and SDs in ESG fluorescence intensity and ESG focal degradation sizes were based on preliminary data, and results were aggregated from the literature. An analysis of variance with an appropriate Bonferroni post hoc test was performed with NCSS (NCSS9 software; NCSS LLC), considering $P \leq 0.05$ to be statistically significant. A log-rank test was performed for analysis of survival curves (NCSS9 software; NCSS LLC), considering $P \leq 0.05$ as statically significant.

Results

Analysis of Organellar Trafficking in Endothelial Cells Subjected to LPS

Under basal conditions, endothelial cells labeled with lysotracker displayed Brownian movement of lysosomes. Application of LPS resulted in agitated lysosomal movement already after several minutes. Figure 1 shows the traces of several lysosomes (different colors indicate different lysosomes) under control and various treatments. Figure 2A shows representative traces of lysosomes over the course of 60 minutes under different conditions. Movement was traced in intervals of 2 minutes. The total length that a lysosome travels is defined as the mean square of the distance, which is the summation of the square of the distance in each step a lysosome travels during a specific time period (each step takes 2 minutes). The mean square of the distance is a commonly held mathematical relation, accounting for time, random motion, and vector distance. The purpose of squaring the distance is to avoid canceling out a distance that a particle travels in the opposite direction during an observed time period. The total length of the LPS group showed a significant increase compared with the control group, starting from 10 minutes ($P < 0.05$) (Figure 2B). The vector distance (square of the distance from the start point of the track to the end point) of the LPS group was significantly increased compared with control, indicating directional movement (Figure 2C). Pretreatment of endothelial cells with the medium conditioned by EPCs, at dilutions 1:10 and 1:50, significantly prevented LPS-induced lysosomal motility. This effect could be mimicked by the pretreatment with a donor of NO, NOHA (Figure 2, A–C).

The motility of the peripherally located lysosomes differed across the treatments, as illustrated by the representative traces (Figure 2A). The trajectories of peripheral lysosomes showed significantly longer distances during the same period of time (the time from one point to another is 2 minutes) in LPS-treated cells than those of the LPS + EPC-CM10 (and to a lesser degree EPC-CM50) or LPS + NOHA groups.

Remarkably, these differences were observed already after 10 minutes ($P < 0.05$) (Figure 2, B and C). The observed changes in motility were preceded by the surge in production of superoxide radicals, as detected with the use of dihydroethidium fluorescence. Application of LPS

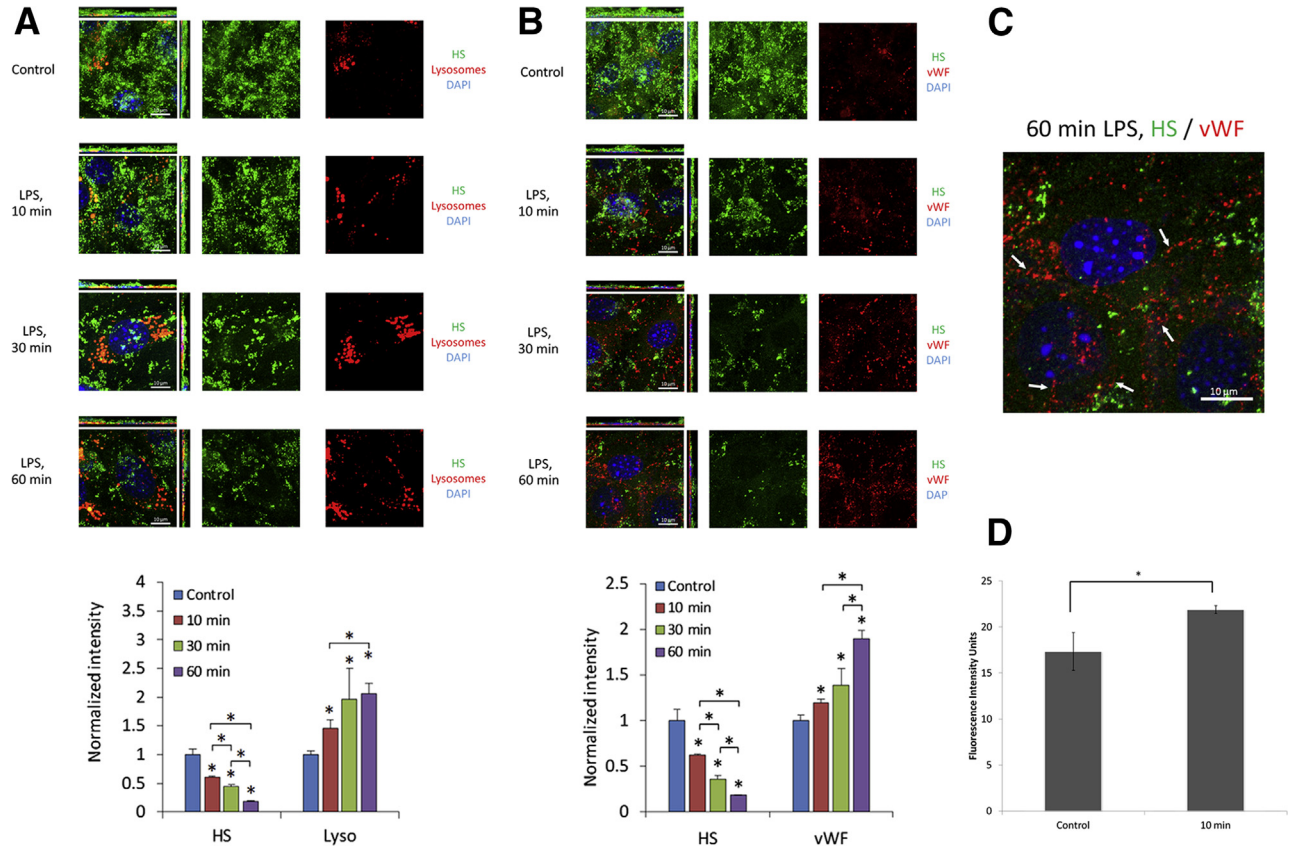

Figure 4 Images of fluorescence-labeled HS (green) and lysotracker (red) (**A**) or vWF/WPB (red) (**B**) under control and after 10, 30, and 60 minutes of exposure to LPS. The cell nuclei were labeled with DAPI (blue). Experiments were performed with bEnd3 endothelial cells that preserve glycocalyx in culture. Relative intensity of anti-HS and lysotracker or vWF/WPBs compared with the control was shown in the bottom of **A** and **B**. **C:** Zoomed image of relative relations between ESG labeled for HS and vWF after 60 minutes of exposure to LPS. Note string-like externalized vWF (**arrows**). **D:** Cathepsin B intensity at baseline and 10 minutes after application of LPS. Data are expressed as means ± SD (**A** and **B**) or means ± SEM (**D**). $n = 3$ samples each for the control and LPS treatment at each time. Five regions of approximately 50 μm × 50 μm were observed in each sample. $^*P < 0.05$ versus control or as indicated in the plot. ESG, endothelial surface glycocalyx; HS, heparan sulfate; LPS, lipopolysaccharide; vWF/WPB, von Willebrand factor-labeled Weibel-Palade body.

resulted in an upstroke of fluorescence intensity already within 5 minutes (Figure 2D).

Analysis of the Early Loss of Endothelial Glycocalyx

Having established the rapidity of LPS-induced exocytosis of peripheral lysosomal pool and demonstrating the ability of EPC-CM or NOHA to halt it, we next addressed a critical question: How early after application of LPS is the loss of ESG detected?

STORM microscopy is characterized by its super-resolution to discern detailed structures and distributions at approximately 20 nm horizontal and approximately 50 nm vertical resolution. Results obtained with STORM are summarized in Figure 3. It provides representative images of ESG in control and 10-minute LPS-treated cells costained with antibodies to vWF. For the control group (Figure 3A), ESG was richly represented by fluorescently labeled anti-HS antibody. However, after 10 minutes of LPS treatment, vWF became externalized and was surrounded by the halo areas of lost HS-decorated ESG. Such a nano-scaled picture for the ESG and exocytotic vWF/WPBs was first observed because of the super-resolution STORM. Figure 3B demonstrates the relative intensity of anti-HS and vWF/WPBs after LPS treatment compared with the control. It indicates that after 10 minutes of LPS treatment, HS decreases to approximately one-third, whereas vWF increases to greater than twofold of their control values, respectively.

With the use of confocal microscopy, similar results were obtained. Figure 4A illustrates (two-dimensional intensity distribution) the loss of ESG at the sites where lysosomal markers are detected in nonpermeabilized cells. The same was true for vWF and HS staining when analyzed by the confocal microscopy (Figure 4B). The relative intensity of the HS decreased when the time of LPS treatment increased, whereas the relative intensity of lysosomes and vWF/WPBs increased (Figure 4, A and B). The longer the length of LPS treatment, the more was the ESG loss and detected exocytosis of lysosomes and vWF/WPBs. The enlarged view in Figure 4C shows string-like externalized vWF; no colocalization of HS and vWF markers was found. Increased levels of cathepsins in the media were found after 10 minutes of LPS treatment (Figure 4D), confirming the exocytosis of

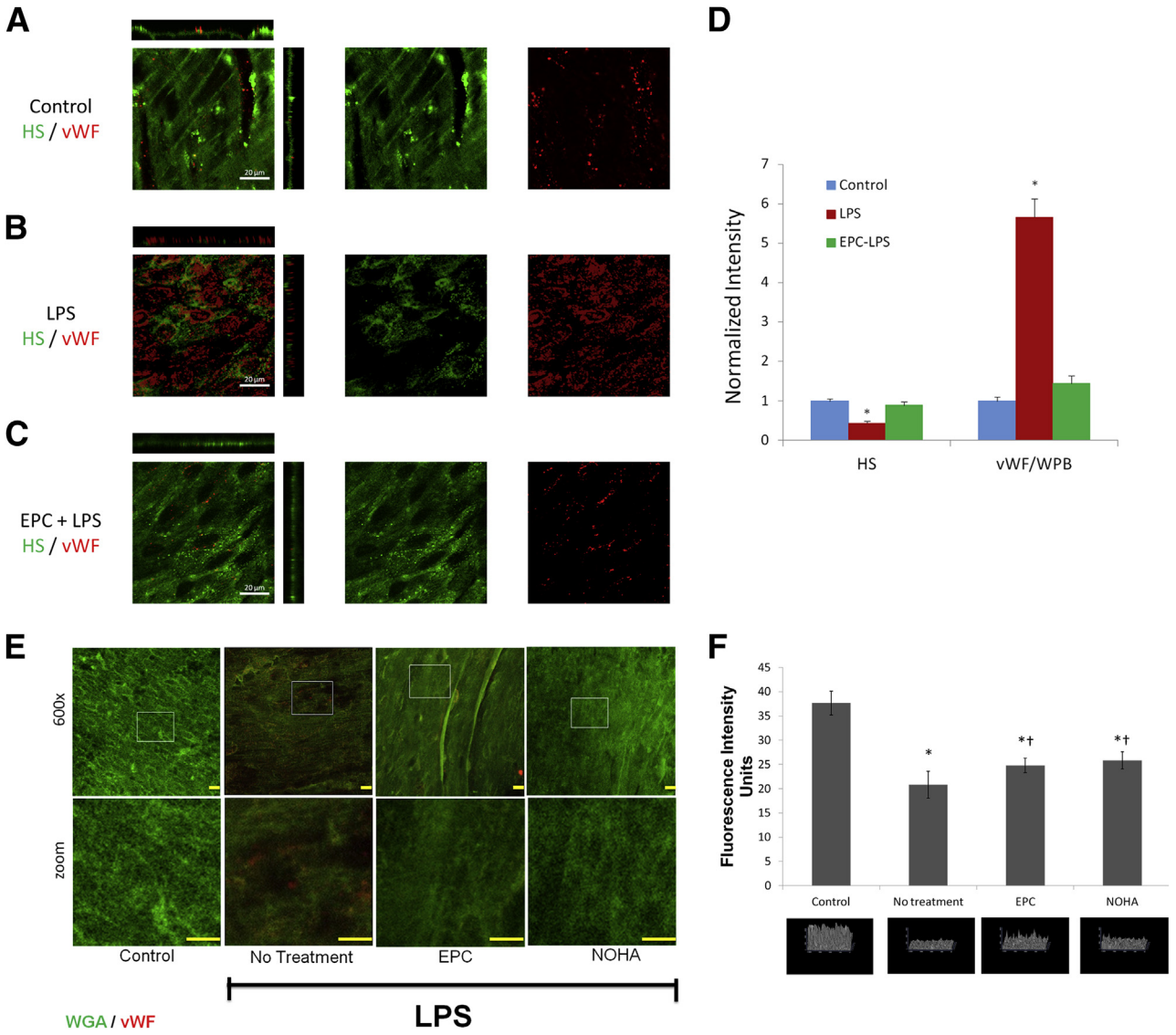

Figure 5 Images of fluorescence-labeled HS (green) and vWF/WPBs (red) of mouse aorta under control (**A**), after IP injection of 5 μg/kg LPS for 60 minutes (**B**), and after EPC pretreatment and IP injection of LPS for 60 minutes (**C**), respectively. **D:** Normalized intensity of HS and vWF/WPBs under control and after LPS treatment with and without EPC pretreatment. **E:** Representative images of *en face* aorta labeled with FITC-WGA obtained 10 minutes after treatment of mice with LPS with or without NOHA or EPC. **F: Upper panel** demonstrates intensity difference across treatments, whereas the **lower panels** depict 3D reconstruction of ESG. Data are expressed as means ± SEM. $n = 6$ control (**D**); $n = 9$ after LPS treatment with and without EPC pretreatment (**D**); $n = 10$ (**F**). $^{*}P < 0.05$ (**D**); $^{*}P < 0.05$ versus control, and $^{\dagger}P < 0.05$ versus LPS alone (**F**). Scale bars: 20 μm (**D**); 10 μm (**E**). EPC, endothelial progenitor cell; FITC, fluorescein isothiocyanate; HS, heparan sulfate; LPS, lipopolysaccharide; NOHA, NG-hydroxy-L-arginine; vWF/WPB, von Willebrand factor-labeled Weibel-Palade body; WGA, wheat germ agglutinin; 3D, three-dimensional.

lysosomes because the fluorescent cathepsin substrate was activated to fluoresce only in the presence of extracellular cathepsin.

Similar results were documented *in vivo* after administration of LPS (Figure 5). Labeling of ESG and vWF in nonpermeabilized mouse *en face* preparations of aorta showed minimal staining for vWF in control, abundant decoration of vWF after the LPS (Figure 5, A and B), and its reduction after EPC (Figure 5, C–F) or NOHA pretreatments (Figure 5, E and F). Please note, *in vivo* EPC treatments used embedded hydrogels, whereas *in vitro* experiments relied on CM. The use of an EPC implantation system provided a consistent, safe, and reliable avenue of delivery for the *in vivo* model that was unattainable through CM. At the same time, ESG was well preserved in control and treated mice (receiving either EPC or NOHA) but was partially depleted in LPS-injected mice (Figure 5F).

Next, we analyzed the density of ESG and the size of areas lacking it with the use of a software program Circle packing. Results confirmed the above observations that LPS induced a significant patchy loss of ESG within 10 minutes of its application, whereas NOHA or EPC-CM treatments prevented this process (Figure 6). The data are consistent with the hypothesis that explained the localized loss of ESG by exocytosis of WPBs and lysosomes.

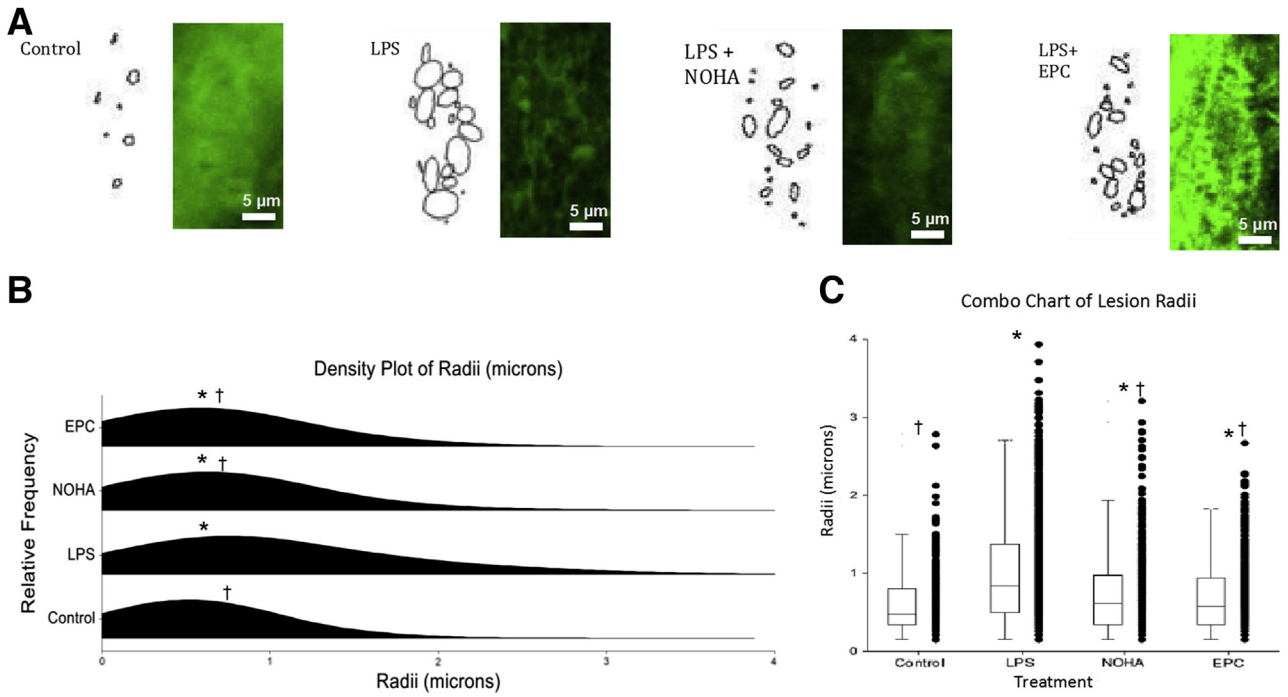

Figure 6 Analysis of the density of the glycocalyx in cultured endothelial cells exposed for 10 minutes to LPS with and without treatments. **A:** An analyzed cell from each group is shown on the left, adjacent to its respective image obtained with the use of the 2D Circle packing algorithm of ImageJ. The algorithm created space-filling ellipses and circles to highlight areas depleted of glycocalyx. **B** and **C:** The distribution plots in **B** and the box and whisker plots in **C** show a statistically significant difference between the mean of the control group and the means of the three experimental groups. In both **B** and **C**, the mean radius of NOHA and EPC-CM are similar and are statistically smaller than that of LPS, representing smaller lesions in the two treatments. $n = 40$ to 50. $^{*}P < 0.05$ versus control, $^{\dagger}P < 0.05$ versus LPS. Original magnification, ×63. CM, conditioned medium; EPC, endothelial progenitor cell; LPS, lipopolysaccharide; NOHA, NG-hydroxy-L-arginine; 2D, two-dimensional.

Long-Term Effects of Preventing ESG Loss on LPS-Induced Multiorgan Failure

To gain further insight into the long-term outcome of preventing exocytosis of lysosome-related organelles during early sepsis, we next examined survival experiments in septic mice. Injection of LPS did not result in a consistent mortality of experimental mice; therefore, we elected to use another model of sepsis, CLP, alone or in combination with NOHA or EPC-CM. The effects of therapeutic maneuvers on the survival of mice with severe sepsis are summarized in Figure 7. The 50% mortality in this model occurred within the first 24 hours. In contrast, treatments with NOHA or EPC-CM significantly delayed and reduced mortality (septic mice were not observed after 72 hours to avoid unnecessary suffering in this nonsurvival model of sepsis). These data support the hypothesis that preventing exocytosis of lysosome-related organelles and patchy loss of ESG early in the course of endotoxemia affords beneficial long-term sequelae in sepsis.

Discussion

Data presented herein demonstrate that LPS triggers, within minutes, a surge in reactive oxygen species (Figure 2E) and exocytosis of WPBs and lysosomes (Figures 3–5). vWF, barely detectable in nonpermeabilized control cells, becomes readily exposed to the antibodies after stimulation with LPS. This is associated with a colocalized loss of ESG, as revealed by confocal microscopy and the first demonstration of this phenomenon by STORM. Blockade of exocytosis prevents the early loss of ESG and may play a role in improving the overall survival of mice with sepsis.

The mechanisms responsible for the loss of glycocalyx have not been exhaustively studied. Two scenarios were

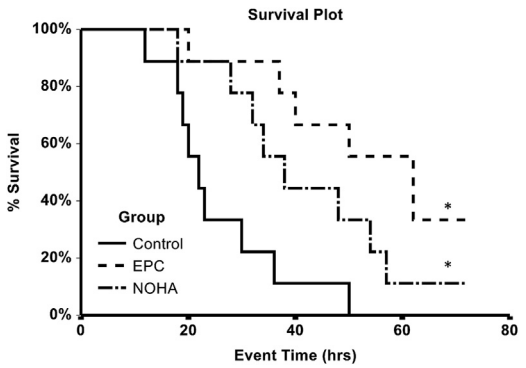

Figure 7 Kaplan-Meyer survival curve (time in hours) of mice with the cecal ligation puncture model of sepsis and the effects of pretreatments that reduce early exocytosis of lysosome-related organelles on long-term survival. $n = 10$ in each group. $^{*}P < 0.05$. EPC, endothelial progenitor cell; NOHA, NG-hydroxy-L-arginine.

proposed. Schmidt et al[17] proposed that its shedding occurs as a result of liberation of heparanase. These studies disclose only one part of the problem—degradation of heparan sulfate moieties, which, however, were shown to be dispensable for the maintenance of the barrier properties of glycocalyx.[18] Annecke et al[19] proposed that the loss of glycocalyx is initiated by the purine metabolite-induced degranulation of resident mast cells and release of tryptase β acting as a sheddase. The instantaneous dilution of tryptase β in the bloodstream should, however, reduce the impact of this factor on ESG. Hence, neither explanation appears to be overarching. Surprisingly, there is no published data on the third possible explanation for the stress-induced loss of glycocalyx, as proposed here, namely, that the exocytosis of WPBs and lysosomes that contain proteolytic, hydrolytic, and glycolytic enzymes is responsible for the initiation of disintegration of glycocalyx. Do potential mediators of exocytosis of WPBs and lysosomes responsible for such an early loss of ESG follow the similar time course? Increased superoxide production by cultured endothelial cells and agitation of exocytosis of lysosomes occurred within minutes after application of LPS (Figure 2). Collectively, these findings provide sufficient support to catalyze further exploration of the proposed hypothesis.

Both lysosomal and WPB compartments are calcium sensitive, and in endothelial cells this process can be blocked by NO, calcium chelators,[16] a 22-amino acid *N*-ethylmaleimide (NEM)-sensitive factor fused to a Tat-carrier peptide,[20] NEM itself, a dominant-negative Ral variant,[21] and a glycine-(Nα-Et)lysine-proline-arginine (ITF 1697) peptide.[22,23] By pharmacologically manipulating exocytosis of these organelles and examining the integrity of glycocalyx in response to stressors we obtained the key test results for the proposed hypothesis.

Matsushita et al[24] developed fusion polypeptides composed of a 22-amino acid NEM-sensitive factor, a regulator of exocytosis, and a carrier peptide derived from the HIV trans-activating regulatory protein domain and demonstrated that inhibition of WPB exocytosis decreased leukocyte trafficking and peritonitis.[20] NEM itself is also a potent inhibitor of exocytosis. de Leeuw et al[21] demonstrated that a small GTP-binding protein, Ral, is involved in exocytosis of WPBs and that expression of a dominant-negative Ral variant prevented it. Bertuglia et al[22] explored a lysine-proline motif encountered in several biologically active small peptides and synthesized a glycine-(Nα-Et)lysine-proline-arginine (ITF 1697) peptide, with the biological half-life of 20 to 120 minutes, and demonstrated that it inhibits ischemia-reperfusion—induced exocytosis of WPBs and protected pulmonary microcirculation by preventing increase in permeability, leukocyte and platelet adhesion, P-selectin, and vWF secretion. This peptide has in its core the Lys-Pro-motif found in tuftsin (a γ-globulin—derived peptide stimulator of phagocytosis), a C-terminal region of α-melanocyte—stimulating hormone endowed with anti-inflammatory properties, and an IL-1β—derived peptide antagonist of hyperalgesic effect of the parent molecule. We reported the use of ITF 1697 in ischemia-reperfusion model of renal injury, confirmed its inhibitory action on exocytosis of WPBs, and demonstrated that the peptide salvages renal function and structural characteristics after renal ischemic injury.[23]

We elected to use NOHA as nitric oxide donor for the following reasons. NOHA is a naturally occurring intermediate product of endothelial nitric oxide synthase that is metabolized to nitric oxide, thus serving as its donor.[25,26] We used the concentration of NOHA that in preliminary studies showed no induction of hypotension or oxidative stress (not shown). Indeed, *in vitro* studies demonstrated that NOHA suppresses vectorial movements of lysosomes after the application of LPS (Figure 2). As demonstrated by Lowenstein's group,[24] NO nitrosylates critical cysteine residues of NEM-sensitive factor and thus inhibits exocytosis of WPBs. Endogenous endothelial NOS becomes uncoupled by oxidative stress early in sepsis, thus contributing to generation of peroxynitrite and deficiency of NEM nitrosylation. Despite using a concentration of NOHA that exhibited no pressor or oxidative effects, we cannot fully exclude the possibility of hemodynamic stabilization and oxidative scavenging that contributed to the significant *in vivo* observations.

The choice of the second therapeutic modality, EPC-CM, is based on previous observations from several groups, including ours, that EPCs exert a protective effect in sepsis.[14] Indeed, according to data presented here, the observed benefits of EPCs could be attributed at least in part to their paracrine effect, resulting in the preservation of ESG. The precise mechanism of this beneficial effect awaits elucidation.

In summary, the above-mentioned studies provide the first demonstration of the early patchy disintegration of ESG which can be prevented by pretreatment with NOHA and EPC-CM, maneuvers that reduced exocytosis of lysosomal-related organelles. Data support the hypothesis assigning to stress-induced exocytosis of these organelles the role of a hair-trigger for local degradation of ESG, a well-known prerequisite for leukocyte infiltration and increase in vascular permeability, which partially accounts for the later mortality in sepsis.

Acknowledgment

We thank Dr. Antonis K. Hatzopoulos (Vanderbilt University, Nashville, TN) for endothelial progenitor cells.

References

1. Aird WC: The role of the endothelium in severe sepsis and multiple organ dysfunction syndrome. Blood 2003, 101:3765—3777
2. Morrison DC, Ulevitch RJ: The effects of bacterial endotoxins on host mediation systems. A review. Am J Pathol 1978, 93:526—618
3. Ratliff BB, Rabadi MM, Vasko R, Yasuda K, Goligorsky MS: Messengers without borders: mediators of systemic inflammatory response in AKI. J Am Soc Nephrol 2013, 24:529—536

4. Kuo MC, Patschan D, Patschan S, Cohen-Gould L, Park HC, Ni J, Addabbo F, Goligorsky MS: Ischemia-induced exocytosis of Weibel-Palade bodies mobilizes stem cells. J Am Soc Nephrol 2008, 19: 2321−2330
5. Reitsma S, Slaaf DW, Vink H, van Zandvoort MA, oude Egbrink MG: The endothelial glycocalyx: composition, functions, and visualization. Pflügers Arch 2007, 454:345−359
6. Becker BF, Chappell D, Jacob M: Endothelial glycocalyx and coronary vascular permeability: the fringe benefit. Basic Res Cardiol 2010, 105: 687−701
7. Cai B, Fan J, Zeng M, Zhang L, Fu BM: Adhesion of malignant mammary tumor cells MDA-MB-231 to microvessel wall increases microvascular permeability via degradation of endothelial surface glycocalyx. J Appl Physiol (1985) 2012, 113: 1141−1153
8. Chappell D, Heindl B, Jacob M, Annecke T, Chen C, Rehm M, Conzen P, Becker BF: Sevoflurane reduces leukocyte and platelet adhesion after ischemia-reperfusion by protecting the endothelial glycocalyx. Anesthesiology 2011, 115:483−491
9. Fu BM, Tarbell JM: Mechano-sensing and transduction by endothelial surface glycocalyx: composition, structure, and function. Wiley Interdiscip Rev Syst Biol Med 2013, 5:381−390
10. van den Berg BM, Vink H, Spaan JA: The endothelial glycocalyx protects against myocardial edema. Circ Res 2003, 92: 592−594
11. VanTeeffelen JW, Brands J, Vink H: Agonist-induced impairment of glycocalyx exclusion properties: contribution to coronary effects of adenosine. Cardiovasc Res 2010, 87:311−319
12. Hatzopoulos AK, Folkman J, Vasile E, Eiselen GK, Rosenberg RD: Isolation and characterization of endothelial progenitor cells from mouse embryos. Development 1998, 125:1457−1468
13. Committee for the Update of the Guide for the Care and Use of Laboratory AnimalsNational Research Council: Guide for the Care and Use of Laboratory Animals. Eighth Edition. Washington, DC, National Academies Press, 2011
14. Ghaly T, Rabadi MM, Weber M, Rabadi SM, Bank M, Grom JM, Fallon JT, Goligorsky MS, Ratliff BB: Hydrogel-embedded endothelial progenitor cells evade LPS and mitigate endotoxemia. Am J Physiol Renal Physiol 2011, 301:F802−F812
15. Yen W, Cai B, Zeng M, Tarbell JM, Fu BM: Quantification of the endothelial surface glycocalyx on rat and mouse blood vessels. Microvasc Res 2012, 83:337−346
16. Matsushita K, Morrell CN, Cambien B, Yang S, Yamakuchi M, Bao C, Hara MR, Quick RA, Cao W, O'Rourke B: Nitric oxide regulates exocytosis by S-nitrosylation of N-ethylmaleimide-sensitive factor. Cell 2003, 115:139−150
17. Schmidt EP, Yang Y, Janssen WJ, Gandjeva A, Perez MJ, Barthel L, Zemans RL, Bowman JC, Koyanagi DE, Yunt ZX, Smith LP, Cheng SS, Overdier KH, Thompson KR, Geraci MW, Douglas IS, Pearse DB, Tuder RM: The pulmonary endothelial glycocalyx regulates neutrophil adhesion and lung injury during experimental sepsis. Nat Med 2012, 18:1217−1223
18. Zhang M, Schekman R: Cell biology. Unconventional secretion, unconventional solutions. Science 2013, 340:559−561
19. Annecke T, Fischer J, Hartmann H, Tschoep J, Rehm M, Conzen P, Sommerhoff CP, Becker BF: Shedding of the coronary endothelial glycocalyx: effects of hypoxia/reoxygenation vs ischaemia/reperfusion. Br J Anaesth 2011, 107:679−686
20. Morrell CN, Matsushita K, Lowenstein CJ: A novel inhibitor of N-ethylmaleimide-sensitive factor decreases leukocyte trafficking and peritonitis. J Pharmacol Exp Ther 2005, 314:155−161
21. de Leeuw HP, Fernandez-Borja M, Reits EA, Romani de Wit T, Wijers-Koster PM, Hordijk PL, Neefjes J, van Mourik JA, Voorberg J: Small GTP-binding protein Ral modulates regulated exocytosis of von Willebrand factor by endothelial cells. Arterioscler Thromb Vasc Biol 2001, 21: 899−904
22. Bertuglia S, Ichimura H, Fossati G, Parthasarathi K, Leoni F, Modena D, Cremonesi P, Bhattacharya J, Mascagni P: ITF1697, a stable Lys-Pro-containing peptide, inhibits weibel-palade body exocytosis induced by ischemia/reperfusion and pressure elevation. Mol Med 2007, 13:615−624
23. Yasuda K, Vasko R, Hayek P, Ratliff B, Bicer H, Mares J, Maruyama S, Bertuglia S, Mascagni P, Goligorsky MS: Functional consequences of inhibiting exocytosis of Weibel-Palade bodies in acute renal ischemia. Am J Physiol Renal Physiol 2012, 302:F713−F721
24. Matsushita K, Morrell CN, Lowenstein CJ: A novel class of fusion polypeptides inhibits exocytosis. Mol Pharmacol 2005, 67:1137−1144
25. Abdul-Hussain MN, Jia YL, Hussain SN: Mechanisms mediating the vasodilatory effects of N-hydroxy-L-arginine in coronary arteries. Eur J Pharmacol 1996, 305:155−161
26. Cho JY, Dutton A, Miller T, Houk K, Fukuto JM: Oxidation of N-hydroxyguanidines by copper(II): model systems for elucidating the physiological chemistry of the nitric oxide biosynthetic intermediate N-hydroxyl-l-arginine. Arch Biochem Biophys 2003, 417:65−76